NUCL SCI TECH (2018) 29:152
https://doi.org/10.1007/s41365-018-0493-y

Calculation of photon attenuation coefficient and dose rate in concrete with the addition of SiO_2 and $MnFe_2O_4$ nanoparticles using MCNPX code and comparison with experimental results

M. Hassanzadeh[1] · **S. M. Sadat Kiai**[2]

Received: 3 January 2018 / Revised: 10 February 2018 / Accepted: 19 March 2018 / Published online: 26 September 2018

Abstract One of the most important safety features of nuclear facilities is the shielding material used to protect the operating personnel from radiation exposure. The most common materials used in radiation shielding are concretes. In this study, a Monte Carlo N-Particle eXtended code is used to calculate the gamma-ray attenuation coefficients and dose rates for a new concrete material composed of $MnFe_2O_4$ nanoparticles, which is then compared with the theoretical and experimental results obtained for a SiO_2 nanoparticle concrete material. According to the results, the average relative differences between the simulations and the theoretical and experimental results for the linear attenuation coefficient (μ) in the SiO_2 nanoparticle materials are 6.4% and 5.5%, respectively. By increasing the SiO_2 content up to 1.5% and the temperature of $MnFe_2O_4$ up to 673 K, μ is increased for all energies. In addition, the photon dose rate decreases up to 9.2% and 3.7% for $MnFe_2O_4$ and SiO_2 for gamma-ray energies of 0.511 and 1.274 MeV, respectively. Therefore, it was concluded that the addition of SiO_2 and $MnFe_2O_4$ nanoparticles to concrete improves its nuclear properties and could lead to it being more useful in radiation shielding.

✉ M. Hassanzadeh
m_hassanzadeh1354@yahoo.com;
mhasanzadeh1354@gmail.com

1 Reactor and Nuclear Safety School, Nuclear Science and Technology Research Institute (NSTRI), Tehran, Iran

2 Plasma and Nuclear Fusion Research School, Nuclear Science and Technology Research Institute (NSTRI), Tehran, Iran

Keywords Shielding · Radiation · Concrete · Attenuation coefficient · Photon dose · MCNPX code · SiO_2 and $MnFe_2O_4$ nanoparticles

1 Introduction

Concrete has been used in nuclear facilities for its physical strength and radiation shielding capability. It contains a mixture of low and high atomic number elements and is therefore effective in shielding photons and neutrons. Lead is found to be another suitable option for shielding against X-rays and gamma rays [1–3].

Nowadays, the use of nanoparticles in materials has attracted attention from researchers owing to a variety of features that have led to its use in a large number of applications [3–5]. Nanoparticles are used as a mixture to improve the mechanical and structural strengths of concrete. In general, the physical properties of nanomaterial are different from those of their bulk counterparts, and frequently display new and surprising phenomena, including the hardening of concrete [6, 7]. Tao studied the microstructure and water permeability of concrete incorporated with SiO_2 nanoparticles, herein referred to as nano-SiO_2. He stated that the presence of nanoparticles can improve the resistance to water penetration in concrete specimens [8]. Moreover, an investigation using environmental scanning electron microscopy (ESEM) demonstrated that the concrete microstructure including nano-SiO_2 led to a denser concrete microstructure and improved pore structure [7, 9].

In this study, for the first time, $MnFe_2O_4$ nanoparticles [10, 11] are added to concrete to improve its nuclear properties. The linear and mass attenuation coefficients are calculated using point isotropic gamma-ray sources based on the Monte Carlo N-Particle eXtended (MCNPX) code, and the results obtained were compared with the experimental and theoretical results. In addition, the configuration and materials are simulated using the MCNPX code [12, 13]. Finally, the photon dose rate is calculated for a system of concrete and $MnFe_2O_4$ nanoparticles, herein referred to as nano-$MnFe_2O_4$ and compared to nano-SiO_2 for different gamma-ray energies and weight percentages.

2 Materials and methods

2.1 Materials

2.1.1 Nano-SiO_2

The chemical analysis of Portland concrete and nano-SiO_2 is given by Elsharkawy and Sadawy [1]. Nano-concrete is formed by grinding the commercially available grade Portland concrete at a high energy [7]. Tables 1 and 2 show the concrete sample without nano-SiO_2 and the concrete mixed with a weight percentage of 0.5% CaO in nano-SiO_2, respectively. Table 3 shows the densities of nano-SiO_2 at different weight percentages of SiO_2 nanoparticles [1].

To study the nuclear attenuation properties, the compressive strength of hardened concrete cubic samples ($7 \times 7 \times 7$ cm^3) is considered. A beam from both point and disk isotropic gamma-ray sources of ^{137}Cs, with one line of energy of 0.662 MeV, ^{60}Co, with two lines of energy of 1.17 and 1.33 MeV, and ^{22}Na, with two lines of energy of 0.511 and 1.274 MeV, was used in the MCNPX code. Figure 1 shows the disk gamma-ray source and cubic concrete sample simulated by the MCNPX code. Figure 2a and b shows the tracks of photons obtained from this code for the point and disk gamma-ray sources, respectively.

Table 1 Chemical analysis of Portland concrete, Ref. [1]

Chemical composition	Weight (%)
SiO_2	23.7
Al_2O_3	5.6
Fe_2O_3	3.3
CaO	63.7
MgO	1.4
SO_3	0.2
K_2O	1.2

Table 2 Chemical composition of nano-SiO_2, Ref. [1]

Chemical composition	Weight (%)
CaO	0.5
SiO_2	93.3
Al_2O_3	3.2
Fe_2O_3	1.7
MgO	0.3
SO_3	0.1
K_2O	0.1
N_2O	0.1

Table 3 Effect of SiO_2 nanoparticle weight percentage addition to concrete on density, Ref. [1]

SiO_2 nanoparticle percentage addition	Density (ρ) (g/cm^3)
0.0	2.15
0.5	2.17
1.5	2.30
2.0	2.26

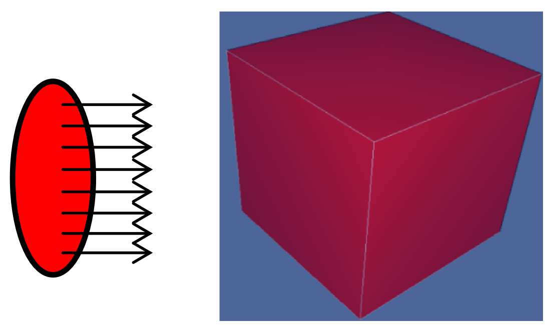

Fig. 1 Disk gamma-ray source and the cubic concrete sample simulated using the MCNPX code (Color online)

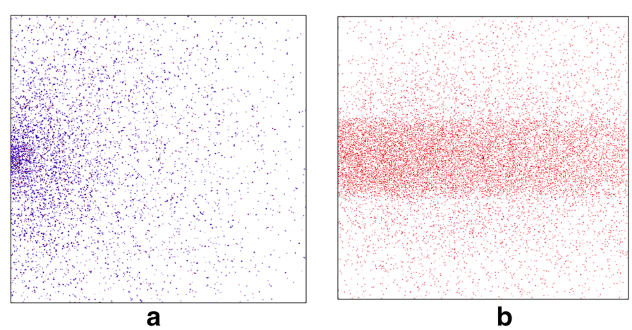

Fig. 2 Tracks of photons simulated using the MCNPX code; **a** point source, **b** disk source (Color online)

2.1.2 Nano-$MnFe_2O_4$

We have added $MnFe_2O_4$ nanoparticles to concrete with a weight percentage of 2.0% CaO at different temperatures, as shown in Tables 4 and 5. $MnFe_2O_4$ is a magnetic oxide, in which oxygen has a close packing structure with the Mn^{2+} and Fe^{3+} ions. These spinel ferrites are very promising candidates for understanding and controlling the magnetic properties of nanoparticles at the atomic level [10, 11].

2.2 Methods

2.2.1 MCNPX code

The shielding material parameters are the most important for characterizing the penetration and diffusion of gamma rays [14]. Theoretical modeling of the photon attenuation coefficients of the materials permits more flexibility and simplicity compared to experimental studies. The linear attenuation coefficients, μ, in materials are determined by the transmission method according to Beer–Lambert's law [1, 14–16]:

$$\mu \cdot X = \ln\left(\frac{I_0}{I}\right), \tag{1}$$

where I_0 and I are the incident and attenuation photon intensities, respectively, μ (cm^{-1}) is the linear attenuation coefficient, and X is the thickness of the slab. The mass attenuation coefficient is defined as μ_m ($cm^2\ g^{-1}$) = μ (cm^{-1})/ρ (g/cm^3).

In this work, the μ and μ_m coefficients are obtained by the MCNPX code at various photon energies: 511, 662, 1170, 1274, and 1332.5 keV. The concrete material content ratios have been defined relative to a sample material in this code. Calculations were performed for one million histories per run using Intel Core i7 CPU 3.40 GHz computers. The obtained statistical errors were $< 1\%$ for a long run time. The flux integrated over a surface tally (F2) has been used in the μ and μ_m calculations [3, 16–18].

Table 4 Composition analysis of nano-$MnFe_2O_4$ concrete

Composition	Weight (%)
CaO	2.0
SiO_2	23.7
Al_2O_3	3.2
Fe_2O_3	1.7
MgO	0.3
SO_3	0.1
K_2O	0.1
N_2O	0.1
$MnFe_2O_4$	68.8

Table 5 Densities of nano-$MnFe_2O_4$ at different temperatures

Temperature (K)	Density (ρ) (g/cm^3)
300	4.373
573	4.773
673	5.194
773	4.745

One of two methods can be used for the calculation of the photon dose rate in concrete samples that are useful for converting the flounce quantities to units of dose. The choice is between using a heating number method or one or more flounces-to-dose conversion functions. Both approaches are valid for photon dose rate calculations, but the use of conversion functions is recommended for dose equivalent and effective dose calculations [13, 19].

In the heating number method, the code calculates the absorbed dose on the basis of the KERMA approximation, which is locally deposited [13]. The KERMA approximation dose can be represented using the following equations:

$$D\left(\frac{\mathrm{Gy}}{\text{Source-particle}}\right) = \frac{C}{N}\sum_{i=1}^{N}\sum_{j=1}^{T}\emptyset\sigma_T(E)H(E), \tag{2}$$

$$C = \left(1.602\times10^{-10}\frac{\mathrm{Gy}}{\mathrm{MeV/g}}\right)\left(1\times10^{-24}\frac{\mathrm{cm}^2}{\mathrm{barn}}\right)\left(\frac{N_a\eta}{M}\right), \tag{3}$$

where N_a is Avogadro's number ($6.022\times10^{23}\ mol^{-1}$), η is the number of atoms per molecule, M is the molar mass in grams, $\emptyset$ is the fluence score in particles/cm^2, σ_T is the total atomic cross section at energy of scoring track in barns, H is the heating number in MeV per collision, T is the number of scoring source particle tracks, and N is the number of source particles.

The second method is the flounce-to-dose conversion function. In this method, the absorbed dose rate is calculated by using DF_n (dose function) and tally F4 operations. Suppose one wanted to compute the dose rate of some type of flux tally, either total or by energy group. This feature allows you to enter a point wise response function (such as flux-to-dose conversion factors) as a function of energy to modify a regular tally. Therefore, the absorbed dose rate is calculated by combining the DF_n and F4 cards. Finally, the DF_n card is defined as follows:

$$DF_n IU\ FAC\ IC\ INT \tag{4}$$

where *IU*, *FAC*, *IC,* and *INT* are the controls units, normalization factor for dose, standard dose function, and energy interpolation, respectively [13, 19].

3 Simulation, experimental, and theoretical results

3.1 Calculation of attenuation coefficients

3.1.1 *Calculation of attenuation coefficients in nano-SiO_2*

The μ value was calculated by the MCNPX code and is shown in Fig. 3. This figure presents the effects of varying gamma-ray energy with μ at weight percentages of 0.0%, 0.5%, 1.5%, and 2.0% SiO_2 in nano-SiO_2 and compares these to the experimental results of Ref. [1]. Calculations have been carried out using a beam of point isotropic gamma-ray sources of ^{137}Cs, with one line of energy of 0.662 MeV, ^{60}Co, with two lines of energy of 1.17 and 1.33 MeV, and ^{22}Na, with two lines of energy of 0.511 and 1.274 MeV. This figure illustrates that the values of μ decrease with increasing gamma-ray energies and that the maximum and minimum values are found at the energies of 0.511 and 1.33 MeV, respectively. In addition, these parameters increase with increasing weight percentage of SiO_2 nanoparticles until 1.5%, after which they decrease due to decreasing density. In general, the relative error in all these calculations is < 1.0%.

3.1.2 *Calculation of attenuation coefficients of nano-$MnFe_2O_4$*

Figure 4 shows the effect of gamma-ray energy on μ for nano-$MnFe_2O_4$ with 2.0% CaO at 300, 573, 673, and 773 K. Figure 5 presents the same effect for nano-$MnFe_2O_4$ at different temperatures, as calculated by the MCNPX code. As shown in Figs. 4 and 5, the values of μ decrease with increasing gamma-ray energies and the maximum and minimum values of μ are found at 0.511 and 1.33 MeV, respectively. In addition, this parameter can be increased by increasing the density up to 5.194 g/cm^3, as seen for the nano-$MnFe_2O_4$ temperature of 673 K.

3.1.3 *Comparison of SiO_2 and $MnFe_2O_4$ nanoparticles*

Figure 6 shows the μ_m of the SiO_2 and $MnFe_2O_4$ nanoparticles constituting 2.0 wt% in concrete for different gamma-ray energies. According to Fig. 6, a fairly good agreement with the experimental results was observed, notably in the simulation of nano-SiO_2 with a density of 2.26 g/cm^3, whereas for the theoretical results, a good agreement was obtained at the density of 2.47 g/cm^3. The average relative differences between the simulation results and the experimental and theoretical results are 6.4%, 5.5%, and 2.1% for the densities of 2.26 g/cm^3 and 2.47 g/cm^3, respectively. Moreover, as seen in this figure, the μ_m of the $MnFe_2O_4$ nanoparticles is much higher compared to that of the SiO_2 nanoparticles, which is attributed to a higher density.

As listed below, there are sources of uncertainty in the results of the MCNPX code in comparison with the experimental and theoretical results:

1. Inherent error in the probabilistic method of the MCNPX code,
2. Inherent error in this code due to the libraries used, especially the inability to define the cross section of the nanoparticles,
3. Physical models used in the MCNPX code.

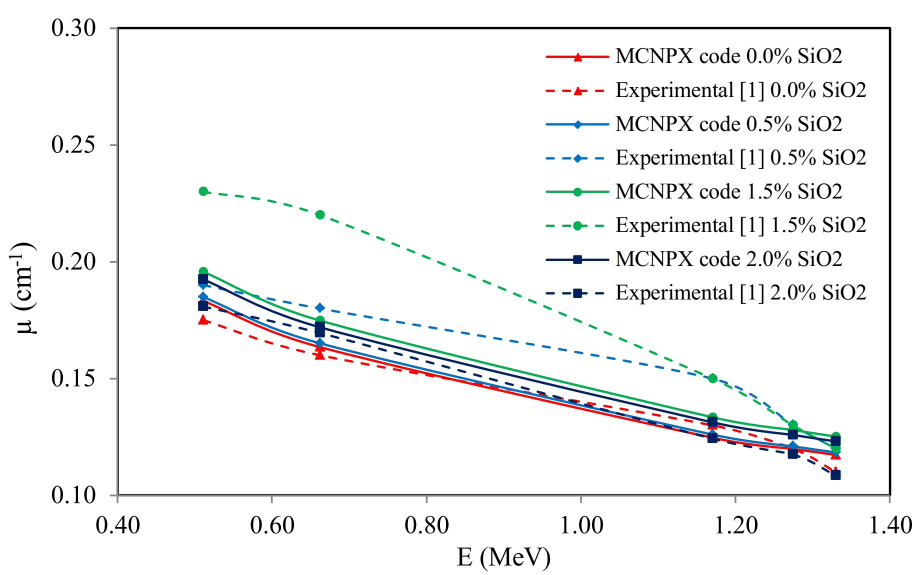

Fig. 3 Effect of gamma energy on the μ at different SiO_2 nanoparticle percentages (Color online)

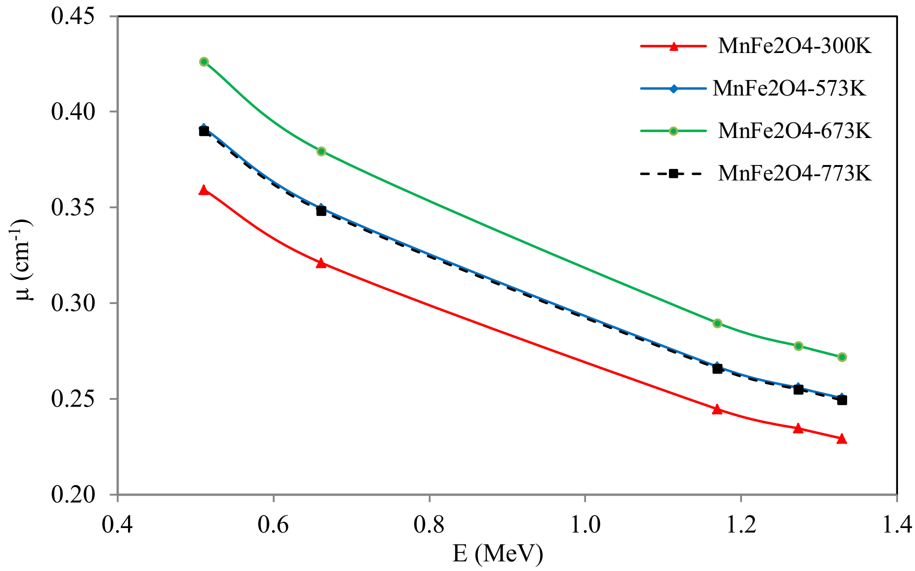

Fig. 4 Effect of gamma energy on μ at different temperatures for nano-$MnFe_2O_4$ (Color online)

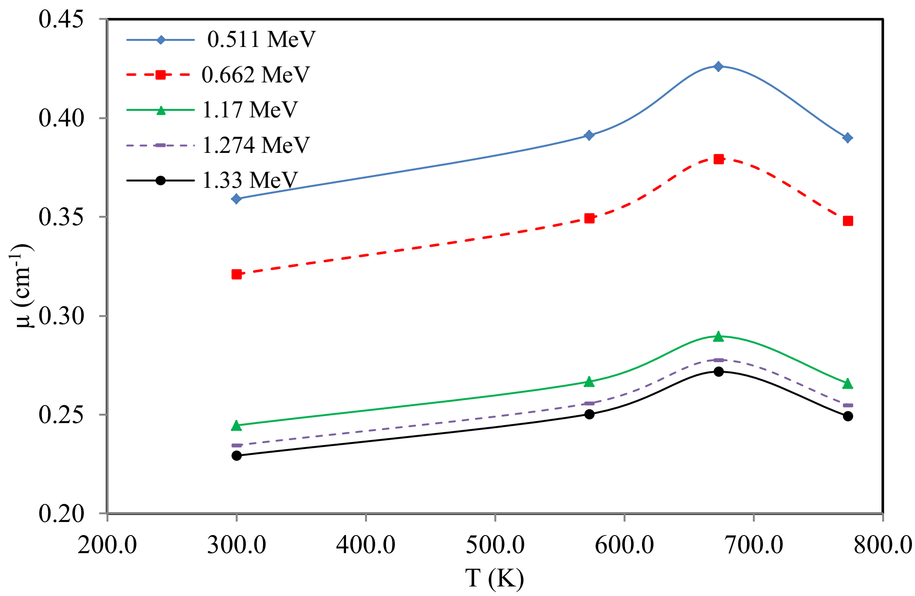

Fig. 5 Effect of temperature of nano-$MnFe_2O_4$ on μ for different gamma energies (Color online)

3.2 Calculation of dose rate

3.2.1 *Calculation of dose rate in nano-SiO_2 and nano-$MnFe_2O_4$ nanoparticles*

Table 6 and Fig. 7 show the effect of adding 2.0 wt% SiO_2 and $MnFe_2O_4$ nanoparticles to concrete on the photon dose rate at different distances from the point source for gamma-ray energies of 0.511 and 1.274 MeV. According to Table 6, the photon dose rate decreases at the average values of about 9.2% and 3.7% for the gamma-ray energies of 0.511 and 1.274 MeV, respectively. This difference is due to the larger μ in nano-$MnFe_2O_4$ in comparison with nano-SiO_2 (as seen in Fig. 6).

4 Discussion and conclusion

Generally speaking, the linear mass attenuation coefficients and photon dose rate of a shielding material depend on the quantity, type, and energy of radiation. It can be shown that most interactions of high energy photons with atoms occur through the Compton Effect, the strength of which depends on the atomic number and amount of primary energy of the gamma source. An increase in photon dose rate can occur owing to Compton reactions involving the photons and the concrete atoms. In addition, photoelectric interactions occur in low energy photons, which is a major mechanism of photon interactions with atoms. Furthermore, there is a greater probability of photon

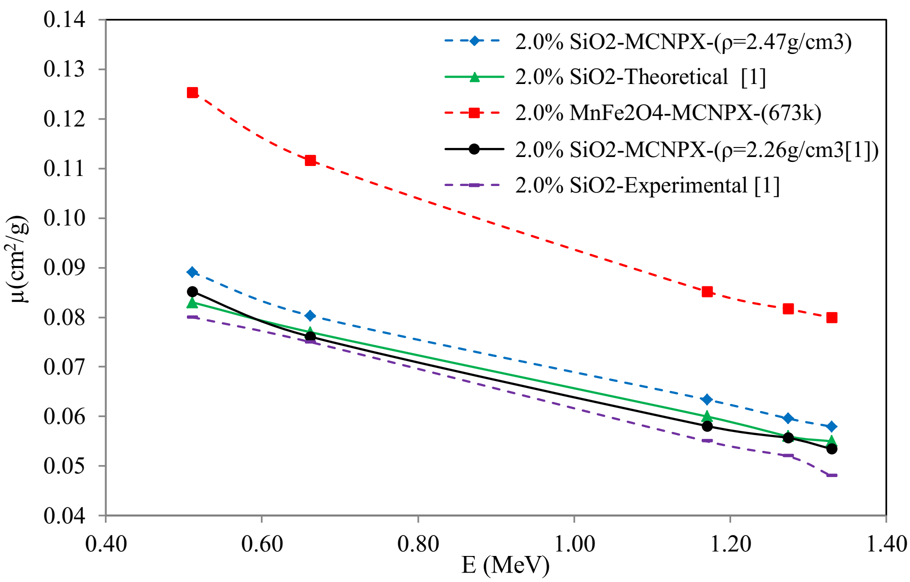

Fig. 6 Comparison of SiO_2 and $MnFe_2O_4$ nanoparticles in concrete on the μ_m at different gamma energies (Color online)

Table 6 Comparison of SiO_2 and $MnFe_2O_4$ nanoparticles in concrete: photon dose rates at different distances from the point source

X (cm)	$MnFe_2O_4$-0.511 MeV	SiO_2-0.511 MeV	Relative difference (%)	$MnFe_2O_4$-1.274 MeV	SiO_2-1.274 MeV	Relative difference (%)
4.0	1.30E−03	1.45E−03	− 11.5	1.75E−03	1.81E−03	− 3.4
5.0	9.76E−04	1.07E−03	− 9.6	1.32E−03	1.37E−03	− 3.8
6.0	7.59E−04	8.27E−04	− 9.0	1.04E−03	1.08E−03	− 3.8
7.0	6.07E−04	6.60E−04	− 8.7	8.40E−04	8.72E−04	− 3.8
8.0	4.98E−04	5.40E−04	− 8.4	6.93E−04	7.19E−04	− 3.8
9.0	4.15E−04	4.50E−04	− 8.4	5.81E−04	6.03E−04	− 3.8
10.0	3.52E−04	3.83E−04	− 8.8	4.95E−04	5.14E−04	− 3.8

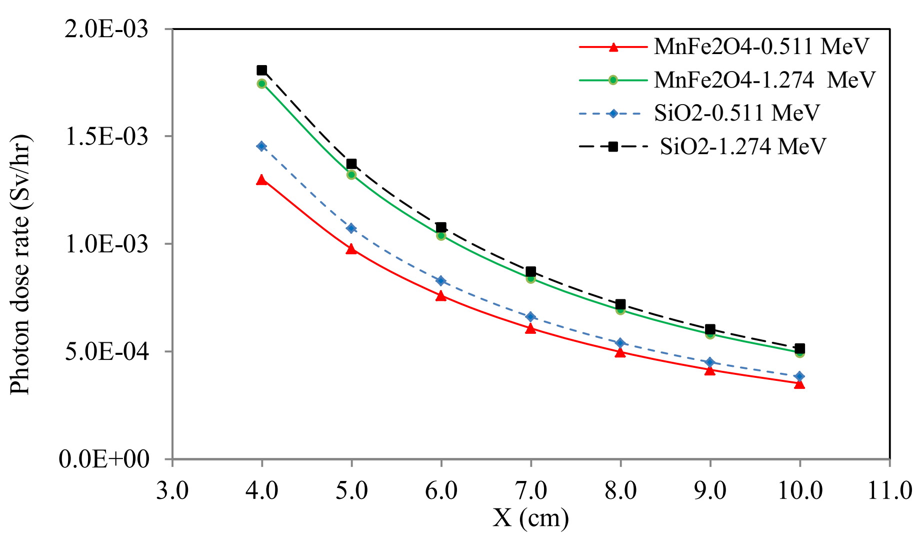

Fig. 7 Comparison of SiO_2 and $MnFe_2O_4$ nanoparticles: the photon dose rate at different distances from the point source (Color online)

interaction at energies much greater than the K- and L-edge energies. When small quantities of nanoparticles are uniformly dispersed in concrete, they act as a nucleus to strongly bind with the concrete hydrates. This leads to a boost in concrete hydration due to their high activity, which is beneficial for the strength of the concrete. While these nanoparticles are bound to the hydrates, they also prevent the crystals from growing, which could lead to a decrease in concrete strength. The loading of the concrete pores with nanoparticles therefore leads to an increase in the strength. Finally, nano-SiO_2 can offer to the hydration process, producing more C–S–H via the formation of $Ca(OH)_2$. In this study, the interaction between a concrete material in a cubic sample configuration and a point isotropic beam for a range of gamma-ray sources has been considered and simulated using the MCNPX code. The μ, μ_m, and photon dose rates have been calculated by this code, from which the statistical errors of the obtained parameters were determined to be less than 1%. According to the obtained μ results, the average relative differences between simulations and the theoretical and experimental results for nano-$MnFe_2O_4$ and nano-SiO_2 were 6.4% and 5.5%, respectively. In addition, the photon dose rate decreases up to 9.2% for nano-$MnFe_2O_4$ and 3.7% for nano-SiO_2 for gamma-ray energies of 0.511 and 1.274 MeV, respectively. Finally, the obtained results are in close agreement with both the experimental and theoretical data. Therefore, it can be stated that the obtained data from this code are a strong tool not only for obtaining μ and μ_m but also for calculating the photon dose rate. It can also be used for future work such as gamma spectroscopy in material characterization, detector design, and especially in investigations of shielding materials for nuclear reactors and high energy therapy facilities.

Acknowledgements The authors are thankful to Dr. Ashoor in the Department of NSTRI for helping to provide the $MnFe_2O_4$ and SiO_2 nanoparticle data.

References

1. E.R. Elsharkawy, M.M. Sadawy, Effect of gamma ray energies and addition of Nano-SiO_2 to concrete on mechanical properties and mass attenuation coefficient. IOSR J. Mech. Civ. Eng. **13**, 17–22 (2016). https://doi.org/10.9790/1684-1306061722
2. I.I. Bashter, Effect of silica fume addition to concrete mixes on radiation attenuation properties. Arab. J. Nucl. Sci. Appl. **34**, 179–189 (2001)
3. H. Tekin, V.P. Singh, T. Manici, Effects of micro-sized and nano-sized WO3 on mass attenauation coefficients of concrete by using MCNPX code. Appl. Radiat. Isot. **121**, 122–125 (2017). https://doi.org/10.1016/j.apradiso.2016.12.040
4. R.S. Chen, Q. Ye, Research on the comparison of properties of hardened concrete paste between Nano-SiO_2 and silica fume added. Concr. J. **1**, 7–10 (2002)
5. Q. Ye, Research on the comparison of pozzolanic activity between Nano-SiO_2 and silica fume. Concr. J. **1**(3), 19–22 (2001)
6. S. Gopinath, P.C. Mouli, A.R. Murthy et al., Effect of nano silica on mechanical properties and durability of normal strength concrete. Arch. Civ. Eng. **4**, 433–444 (2012). https://doi.org/10.2478/v.10169-012-0023-y
7. M.J. Carmichae, G.P. Arulraj, Strength and permeability studies on concrete with nano-cement. IJCIET **8**(1), 132–139 (2017). **(ID: IJCIET_08_01_014)**
8. J. Tao, Preliminary study on the water permeability and microstructure of concrete incorporating Nano-SiO_2. Concr. Concr. Res. **10**(35), 1943–1947 (2005). https://doi.org/10.1016/j.cemconres.2005.07.004
9. I.I. Bashter, A. El-Sayed Abdo, A.S. Makarious et al., A comparative study of the attenuation of reactor thermal neutrons in different types of concrete. Ann. Nucl. Energy **23**, 1189–1195 (1996). https://doi.org/10.1016/0306-4549(95)00122-0
10. Z. Surowiec, M. Wiertel, W. Gac et al., Influence of annealing temperature on structural and magnetic properties of MnFe2O4 nanoparticles. Nukleonika **60**, 137–141 (2015). https://doi.org/10.1515/nuka-2015-0029
11. S. Kanagesan, S.B.A. Aziz, M. Hashim et al., Synthesis, characterization and in vitro evaluation of manganese ferrite (MnFe2O4) nanoparticles for their biocompatibility with murine breast cancer cells (4T1). Molecules (2016). https://doi.org/10.3390/molecules21030312
12. H.O. Tekin, MCNP-X Monte Carlo code application for mass attenuation coefficients of concrete at different energies by modeling 3 × 3 Inch NaI (Tl) detector and comparison with XCOM and Monte Carlo data. Sci. Technol. Nucl. Instal. (2016). https://doi.org/10.1155/2016/6547318
13. D.B. Pelowitz, *MCNPX user's manual, version 2.6.0*, LA-CP-07-1473, Los Alamos National Laboratory (2008)
14. V.P. Singh, S.P. Shirmardi, M.E. Medhat et al., Determination of mass attenuation coefficient for some polymers using Monte Carlo simulation. Vacuum **119**, 1–5 (2015). https://doi.org/10.1016/j.vacuum.2016.11.011
15. M.A. Abdel-Rahman, E.A. Badawi, Y.L. Abdel-Hady et al., Effect of sample thickness on the measured mass attenuation coefficients of some compounds and elements for 59.54, 661.6 and 1332.5 keV γ-rays. Nucl. Instrum. Methods A **447**, 432–436 (2000). https://doi.org/10.1016/S0168-9002(99)01257-7
16. S.M. Vahabi, M. Bahreinipour, M. Shamsaie, A comparison study for mass attenuation coefficients of some amino acids using MCNP code. Kerntechnik **82**, 339–343 (2017). https://doi.org/10.3139/124.110678
17. Y.C. Kam, K.-C. Pei, C.-L. Chang et al., Strength and fracture toughness of heavy concrete with various iron aggregate inclusions. Nucl. Eng. Des. **228**, 119–127 (2004). https://doi.org/10.1016/j.nucengdes.2003.06.008
18. A. Mesbahi, F. Jamali, N. Gharehaghaji, Effect of photon beam energy, gold nanoparticle size and concentration on the dose enhancement in radiation therapy. BioImpacts **3**, 29–35 (2013). https://doi.org/10.5681/bi.2013.002
19. A. Abbasi, M. Hassanzadeh, Measurement and Monte Carlo simulation of γ-ray dose rate in high-exposure building materials. Nucl. Sci. Tech. **28**, 20 (2016). https://doi.org/10.1007/s41365-016-0171-x